Lab on a Chip

ROYAL SOCIETY OF CHEMISTRY

PAPER

View Article Online
View Journal | View Issue

Check for updates

Cite this: *Lab Chip*, 2025, **25**, 2903

CO_2 hydrate nucleation study: novel high-pressure microfluidic devices†

Peyman Dehghani,[ab] Anne Sinquin, *[a] Nicolas Gland, [a] Eric Lécolier,[a] Livio Ruffine[a] and Anh Minh Tang [b]

Received 26th December 2024,
Accepted 28th April 2025

DOI: 10.1039/d4lc01102c

rsc.li/loc

This study presents the development and application of a novel high-pressure microfluidic system for investigating CO_2 hydrate nucleation and growth, with applications for carbon capture and storage (CCS) technologies. Two distinct microchip geometries—a capillary channel chip (serpentine-shaped) and an advanced droplet trap chip— were respectively designed and evaluated. These microchips enable the generation, trapping, and observation of CO_2 droplets or bubbles within aqueous systems under static and dynamic conditions. The capillary channel chip allows droplet storage in a single serpentine channel, whereas the droplet trap chip offers superior immobilization and control, preventing droplet/bubble displacement during CO_2 hydrate formation. High-resolution optical imaging, coupled with precise pressure and temperature regulation and control, facilitated real-time visualization of CO_2 hydrate crystallization at CO_2–water interfaces under varying temperature and pressure conditions. Experimental results reveal the influence of geometry, flow dynamics, and hydrodynamics on hydrate morphology and growth. The high-pressure microfluidic setup provides an adaptable and scalable approach for studying hydrate behavior, offering valuable insights for investigating CO_2 storage in geological formations.

Open Access Article. Published on 29 april 2025. Downloaded on 05-06-2026 21:04:26.
This article is licensed under a Creative Commons Attribution-NonCommercial 3.0 Unported Licence.

1. Introduction

Storing carbon dioxide (CO_2) in depleted oil and gas reservoirs is one of the most promising industrial solutions to mitigate greenhouse gas emissions and combat climate change.[1,2] However, throughout the process—from capture (or production) to final storage—CO_2 undergoes various pressure and temperature conditions, leading to phase transitions between gas, liquid, and even solid states.[3] One significant physical phenomenon that can be observed during CO_2 storage is the Joule–Thomson cooling effect, which occurs when CO_2 expands from high surface to lower reservoir pressures, potentially causing the temperature to drop to sub-zero levels.[3,4] Consequently, this could place the storage environment within the CO_2 hydrate stability zone, potentially forming CO_2 hydrates and thus reducing CO_2 injectivity.[3] Gas hydrates are non-stoichiometric ice-like crystals formed from water and gas under low temperature and high-pressure conditions. These structures consist of hydrogen-bonded water molecules forming polyhedral cavities that trap small gas molecules.[5–7] Conventional methods for studying hydrate formation typically require a high-pressure cell and a significant number of experiments, which are time-consuming and require space and fluid volumes. This highlights the need for more practical and efficient alternatives.

Microfluidics is the study of systems that control fluids at the microscale, typically through microchannels with dimensions ranging from tens to hundreds of micrometers.[8] This technique of investigation is promising for various energy and environmental technologies.[9,10] One significant advantage of the various interplays in gas–liquid and liquid–liquid mixtures is that droplet-based microfluidic devices facilitate the execution of numerous experiments under identical conditions.[8,11] Each droplet is considered as an independent reactor within these systems, with volumes typically in the nanoliter range.[8] Over the past decade, interest in microfluidic crystallization under varying pressure conditions has significantly increased.[12] Under atmospheric pressure conditions, a tool for droplet-based milli-fluidics was developed to study the memory effect on cyclopentane (CP) hydrate crystallization. The experimental setup features a spiral capillary tube at atmospheric pressure, where a train of water droplets is generated by co-injecting water and CP at constant rates through a co-flow junction.[13] Similarly, Dehghani *et al.* investigated the nucleation and growth of CP

[a] *IFP Energies nouvelles, 1-4 Avenue de Bois-Préau, 92852 Rueil-Malmaison, France. E-mail: anne.sinquin@ifpen.fr*
[b] *Navier, ENPC, Institut Polytechnique de Paris, Univ Gustave Eiffel, CNRS, Marne-la-Vallée, France*

† Electronic supplementary information (ESI) available. See DOI: https://doi.org/10.1039/d4lc01102c

Open Access Article. Published on 29 april 2025. Downloaded on 05-06-2026 21:04:26.
This article is licensed under a Creative Commons Attribution-NonCommercial 3.0 Unported Licence.

hydrates using an in-house droplet-based capillary tube (serpentine shape), capable of storing trains of identical water droplets in CP.[14]

Recently, high-pressure microfluidic platforms have been developed to study CO_2 mass transfer, involving the generation of CO_2 droplets/bubbles under reservoir-like conditions.[15] Researchers have utilized microchips with serpentine design to investigate the transport dynamics and mass transfer of CO_2 droplets/bubbles. Ho *et al.* employed a microfluidic setup to investigate the CO_2 mass transfer rate in water under high-pressure conditions, ranging from 2.5 bar (normal ground state) to 95 bar (deep reservoir conditions), across three different phases (gas, liquid, and supercritical).[16] The study determined the liquid-side volumetric mass transfer coefficient to quantify the dynamic CO_2 mass transport.[16] In another study, gas–liquid slug flow was generated at a T-junction with a capillary tube (serpentine shape) to study the bubble dissolution and mass transfer rate under dynamic conditions. Its movement downstream allows determining the sizes of CO_2 bubbles and liquid slugs at pressures up to 30 bar.[17] Recently, Yang *et al.* conducted a microfluidic experiment in the context of carbon sequestration in saline aquifers to investigate CO_2 transport dynamics in brine under reservoir-like conditions (80 bar and 50 °C).[18]

In microfluidic research, glass capillary tubes and chips are widely used to investigate gas hydrate formation and dissociation under high pressure. For instance, the processes of methane hydrate formation and dissociation in a porous medium were observed in a micromodel, where the hydrate phase transition was visually observed, and the relationship between hydrate saturation and permeability was analyzed.[19] A heterogeneous micromodel was used to investigate methane hydrate formation and dissociation in a study from Ji *et al.* Hydrate formation was investigated at the gas–liquid interface.[20] Additionally, Li *et al.* used a porous glass micromodel device to perform direct visual investigations of the crystals' kinetics and morphological evolution during the formation and dissociation processes of methane hydrate in either water or brine.[21] In high-pressure droplet-based research, the study of hydrate formation often focuses on observing individual CO_2 droplets within capillary tubes and records the formation conditions.

Le Goff *et al.* presented and used a glass capillary sealed at one end to determine CO_2 hydrate dissociation temperatures. The experiments were conducted at various pressures and brine concentrations, simulating conditions near the wellbore during CO_2 injection into a depleted reservoir.[22] In another study, the roles of supercooling and wettability were investigated by forming hydrates of CO_2 and N_2 within thin glass capillaries.[23]

Existing methods for droplet-based hydrate formation are limited, and at high pressure focus on CO_2 mass transfer under dynamic conditions or on hydrate formation of a single droplet/bubble under static conditions. Other studies are performed in atmospheric pressure conditions using molecules stabilising hydrate in these atmospheric conditions. Therefore, there is a need to investigate CO_2 hydrate at high pressure in such a way that facilitates the transformation of multiple droplets or bubbles into hydrates. This study aims to develop a microfluidic technique to investigate CO_2 hydrate formation from numerous droplets or bubbles under both static and dynamic conditions. To keep multiple droplets or bubbles immobile, it is necessary to trap or immobilize them at specific locations within the chip once they have been generated. We have considered two experimental techniques to achieve this objective: a capillary channel chip (serpentine-shaped) and a droplet-trapping chip. In the first method, droplets or bubbles of one fluid (CO_2 gas or liquid, or water) in the other fluid are stored under pressure in a channel. Each isolated droplet or bubble acts as a microreactor. In the second method, droplets of one fluid are trapped within specific geometric features, while the other fluid can flow through a bypass channel. This design ensures that the droplets remain immobile and allows experiments under static and dynamic conditions. This setup provides flexibility, enabling three configurations of injections: water and CO_2 are static, one fluid remains static while the other flows dynamically, or both fluids are dynamic.

2. Experimental setup

2.1. Microfluidic platform

In these experiments, deionized (DI) water and CO_2 gas/liquid with 99.99% purity are used to form hydrates. The experiments are conducted on a high pressure/high or low temperature (HP-HLT) microfluidic platform (Fig. 1). This platform features a microfluidic chip and a chip holder; it integrates various tools to streamline fluid injections into the chip, temperature control, back pressure, and an optical observation device. Two syringe pumps (model 65D) are employed for the CO_2 and water injection. These pumps can inject fluids at a flow rate as low as 0.01 μL min^{-1} and withstand pressures up to 1380 bar. The temperature of the

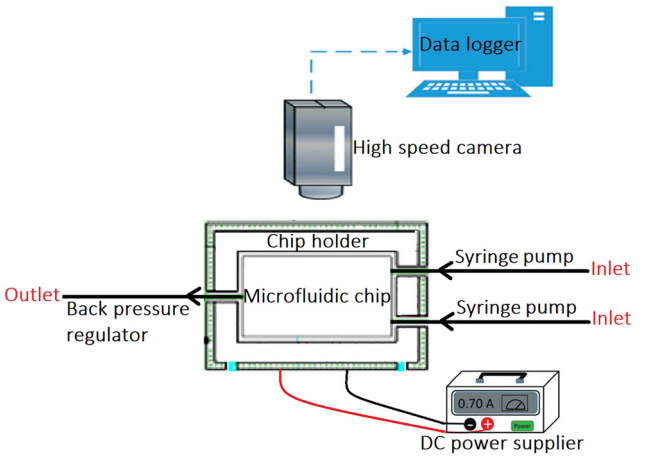

Fig. 1 Diagram of the HP-HLT microfluidic platform.

This journal is © The Royal Society of Chemistry 2025

Open Access Article. Published on 29 april 2025. Downloaded on 05-06-2026 21:04:26.
This article is licensed under a Creative Commons Attribution-NonCommercial 3.0 Unported Licence.

chip is controlled using a Peltier module, (see section 2.3). Additionally, pressure at the outlet is maintained with a back pressure regulator. Various sensors measure key parameters such as pressure, temperature, and flow rate, and all are connected to a data logger. The optical imaging system features an i-Speed 230 camera (iX Cameras Inc.®), capable of recording up to 225 000 frames per second (FPS) at lower resolutions or 2500 FPS at full resolution. Resolution refers to the recording screen's dimensions (width × height). In this study, frame rates of 1, 10, 50, and 100 FPS were used, depending on the recording objective. This camera is mounted on a ZEISS® Stemi 305 binocular microscope, providing magnification ranging from 0.63× to 5×.

2.2. Chip holder

The microfluidic chip must meet several of the following critical requirements:

- Maintain transparency within the chip holder for optical observation,
- Withstand pressures up to 70 bar,
- Allow flexible surface temperature measurement,
- Support cooling to temperatures as low as −20 °C.

To achieve these specifications, an in-house pressurized chip holder was designed, as shown in Fig. 2a. The holder accommodates various connections, including fluid inlets and outlets. Cooling is managed through a Peltier module located between the microchip and a copper-made heat exchanger. Fig. 2b presents a side view of the system, displaying its different components.

2.3. Temperature control

A Peltier module is used to achieve rapid, efficient, and adjustable temperature control of the microfluidic chip. When an electric direct current is applied, this module generates a temperature difference between its hot and cold sides. Directly under the microfluidic chip, the cold side of the Peltier module is installed, and close contact with the chip is maintained. A copper heat exchanger dissipates the heat produced by the Peltier module. Inside the channels of this heat exchanger circulate a mixture of 60% water and 40% methylene glycol, maintained at a required temperature range regulated by a cryo-thermostat. A glycerol pool is incorporated between the chip and the holder to enhance observation and recording with the high-speed camera and prevent water condensation. A surface-specific Pt100 sensor is attached to the surface of the microfluidic chip to measure its temperature (Fig. 3).

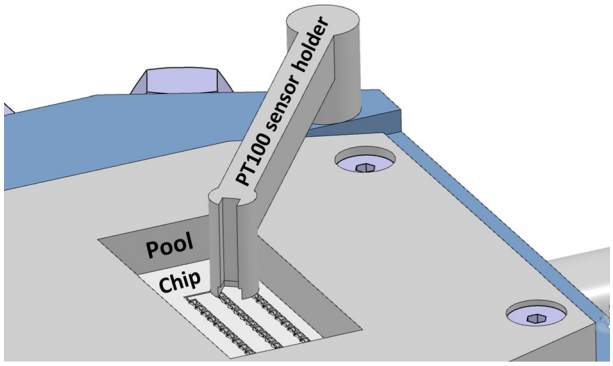

Fig. 3 Temperature measurement system using a surface-specific PT100 sensor. A pool is filled with glycerol to prevent condensation, improve visibility, and enhance temperature uniformity across the surface.

3. Methods

3.1. Method 1: capillary channel chip (serpentine-shaped)

The primary goal was to identify an affordable commercial chip with a high storage capacity to accommodate numerous droplets or bubbles. However, standard T-junction and flow-focusing chips lacked sufficient storage or had storage areas incompatible with our chip holder's observation window. Consequently, a commercially available microchip (Micronit©) was selected. This microchip features a Y-junction for generating CO_2 droplets and bubbles and a serpentine-shaped channel for storing them (Fig. 4a). The channel dimensions are 250 μm in width, 140 μm in height, and 494 mm in total length (Fig. 4b). The chip is made of borosilicate glass (hydrophilic) and is manufactured using an etching technique. To ensure a robust connection capable of withstanding high pressures, the chip is secured with a

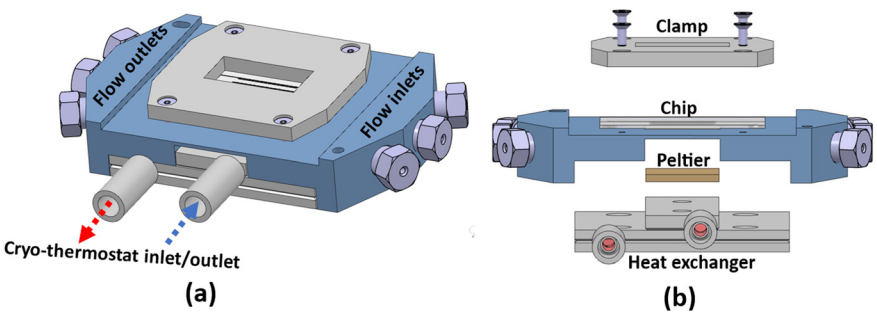

Fig. 2 Two views of the chip holder system: (a) a 3D view showing the flow inlets and outlets, (b) a side view presenting the system's structural details.

Open Access Article. Published on 29 april 2025. Downloaded on 05-06-2026 21:04:26.
This article is licensed under a Creative Commons Attribution-NonCommercial 3.0 Unported Licence.

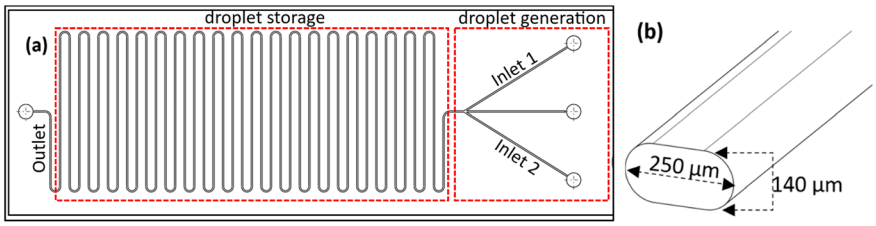

Fig. 4 (a) View of the two sections of the microchip: droplet generation and storage. The inlets and outlet are indicated. In this study, two inlets on the chip are utilized; (b) a 3D view of the channel.

clamp and nuts (Fig. 2), allowing the system to operate under high-pressure conditions.

To form CO_2 hydrate, the following steps are applied.

Step 1: generation of CO_2 droplets/bubbles. Water is introduced into the microfluidic chip channel and pressurized to the desired experimental conditions. The CO_2 pumps, set to the same pressure as the water, are then activated. The two pumps are turned on simultaneously to generate CO_2 droplets or bubbles in water through the Y-junction of the chip. Once droplets or bubbles are formed, the optimal flow rate ratio between the CO_2 and water phases is determined. The light reflection around the temperature sensor is due to the glycerol pool. (Fig. 5). This ensures control over droplet size and maintains consistent spacing between droplets. The microchip temperature is maintained at 11 °C for both CO_2 gas (at 15 bar) and liquid (at 50 bar).

Step 2: immobilization of CO_2 droplets/bubbles. Once droplets/bubbles are generated under dynamic pressure conditions, stopping the CO_2 and water pumps can cause residual flows to enter the channel, potentially destroying the generated droplets/bubbles. Therefore, controlling this residual flow is crucial. A bypass line is installed between the water inlet and the chip outlet (Fig. 6). The bypass valve remains closed during droplet/bubble generation (Fig. 6a). Once the optimal droplet/bubble size is achieved (Fig. 6b), the bypass valve is opened instead of stopping the pumps. This instantaneously discharges the water, and CO_2 inlet flows through the bypass line (Fig. 6c), effectively stopping and preserving the droplets/bubbles within the pressurized channel (Fig. 6d).

Step 3: formation of CO_2 hydrate by cooling. To form CO_2 hydrate, the chip temperature is decreased while the fluid pressure is maintained constant. Significantly, the inlets and outlet are not in direct contact with the Peltier module's cooling zone. During this phase, droplets and bubbles begin to move as the temperature of the storage zone is lowered (Fig. 7). As the temperature decreases, the droplets tend to shift toward the outlet. This can result in several issues: droplet/bubble coalescence and the entering of new droplets/bubbles with different temperatures into the storage zone. Additionally, the size of the droplets/bubbles decreases over time as the temperature drops.

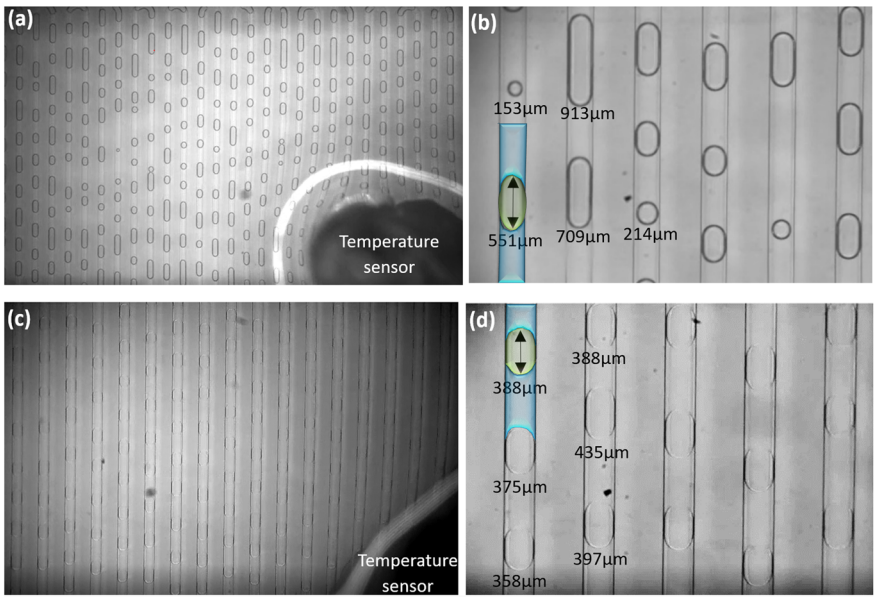

Fig. 5 (a) Storage of approximately 250 CO_2 bubbles (CO_2 gas) in water at a pressure of 15 bar; (b) optical zoom of selected CO_2 bubbles; (c) storage of approximately 150 CO_2 droplets (liquid CO_2) in water at a pressure of 50 bar; (d) optical zoom of selected CO_2 droplets. For better clarity, a sample of CO_2 gas and liquid is colored green, with water on both sides colored blue.

 This journal is © The Royal Society of Chemistry 2025

Open Access Article. Published on 29 april 2025. Downloaded on 05-06-2026 21:04:26.
This article is licensed under a Creative Commons Attribution-NonCommercial 3.0 Unported Licence.

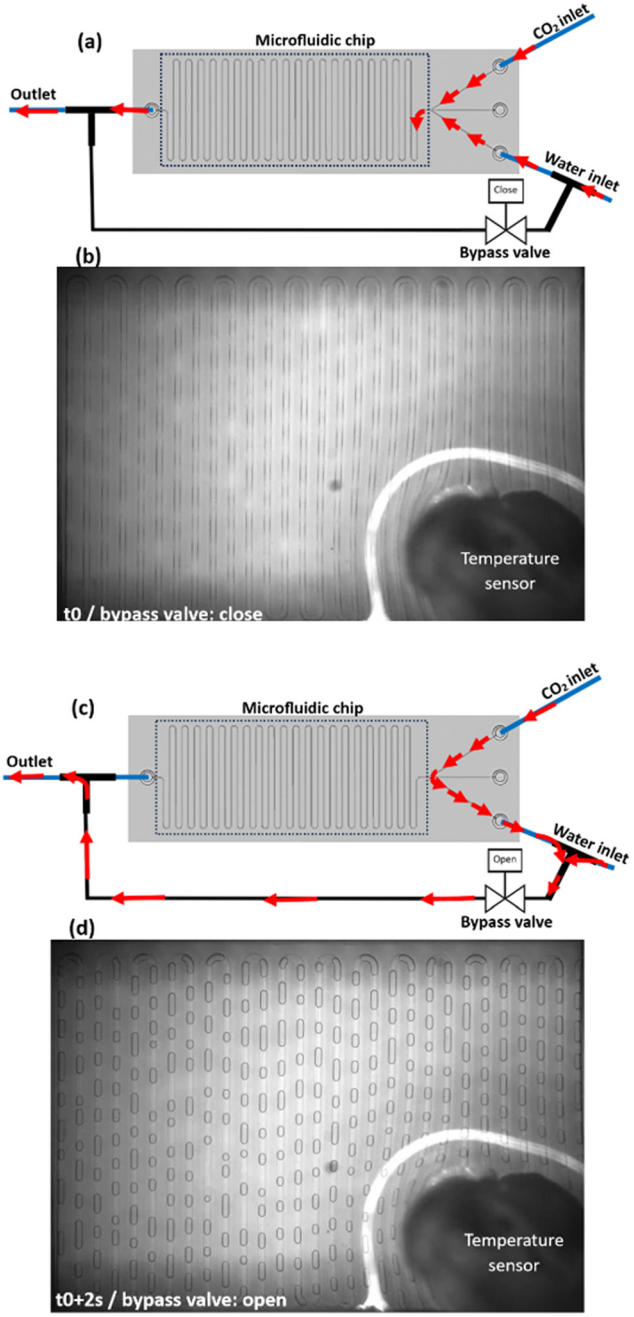

Fig. 6 (a) Schematic view of the microchip and inlets entering the storage zone when the bypass valve is closed; (b) microscopic view of the storage zone with droplets/bubbles in motion (bypass closed); (c) bypass valve opened; (d) view of the storage zone with stopped droplets/bubbles.

To maintain the bubbles or droplets stable throughout the cooling process, two solutions were identified: (1) pre-cooling of the system: it is recommended to pre-cool the storage zone to −10 °C (within the hydrate stability zone) before generating droplets. This minimizes temperature variations and significantly reduces droplet movement; (2) enhancing the chip design: fabricate a modified chip able to trap droplets or bubbles fully. The results of the first solution are presented in section 4.1, while the second solution is explained in the following section.

3.2. Method 2: droplet trap

In a second approach to mitigate the issues observed in the first method, such as droplet/bubble movement, droplet/bubble size variation, and inconsistent spacing between CO_2 and water phases at different locations, a custom-designed chip is required. The new chip must satisfy several key criteria:

- It should efficiently produce uniform droplets/bubbles and be able to stop them without a bypass valve.
- This chip should facilitate monitoring all droplets/bubbles over time, both in static and dynamic conditions.

The storage area should be transparent and compact to enable microscopic observation, like for the first system.

Various methods are available to trap droplets or bubbles in microfluidic systems: surface chemistry modifications to enhance adhesion on channel surfaces, electrowetting to control droplet positions using electric fields, hydrodynamic traps, and geometric traps with physical constrictions or wells to immobilize droplets. In this work, a prototype chip with a specific droplet-trap geometry was initially fabricated. Our design was inspired by a low-pressure microfluidic approach to studies on protein nucleation from the work of D. Radajewski *et al.*[24] After testing different channel sizes at high pressure, the optimal design was selected, and a second chip based on this concept was fabricated.

Design prototype. In this prototype chip, capillary valves were created using different fluid resistances and bypass channels to trap droplets or bubbles from single-phase flow. Fig. 8 illustrates a schematic of this design, featuring two distinct groups of geometries. The chip is made of fused silica (hydrophilic) and manufactured using the selective laser-induced etching (SLE) technique.

Each group consists of two lines, with four distinct lines for testing and determining the optimal droplet trap/restriction diameter ratio. The chip is designed to trap droplets/bubbles, with one phase in trap sections (round sections) and the other in bypass channels. The four lines' differences lie in bypass width, restriction width, and the spacing between traps (see Table 1). After conducting these experiments, it was found that lines L3 and L4 were suitable for both CO_2 gas and liquid. Ultimately, both lines in group 2 provided reliable performances, but the optimal parameters were observed in G2/L3. The geometry of the latter offers the optimal ratio of hydrodynamic resistances between the restriction, trap section, and bypass channel. Notably, the selection of the G2/L3 group as the optimal design was based on qualitative optical observations. While quantitative data would strengthen these conclusions, the qualitative observations provided sufficient guidance for final chip fabrication. The exclusion of other groups was based on observed limitations: G1/L1 (trap diameter), G1/L2 (loop count), G2/L4 (restriction width).

Open Access Article. Published on 29 april 2025. Downloaded on 05-06-2026 21:04:26.
This article is licensed under a Creative Commons Attribution-NonCommercial 3.0 Unported Licence.

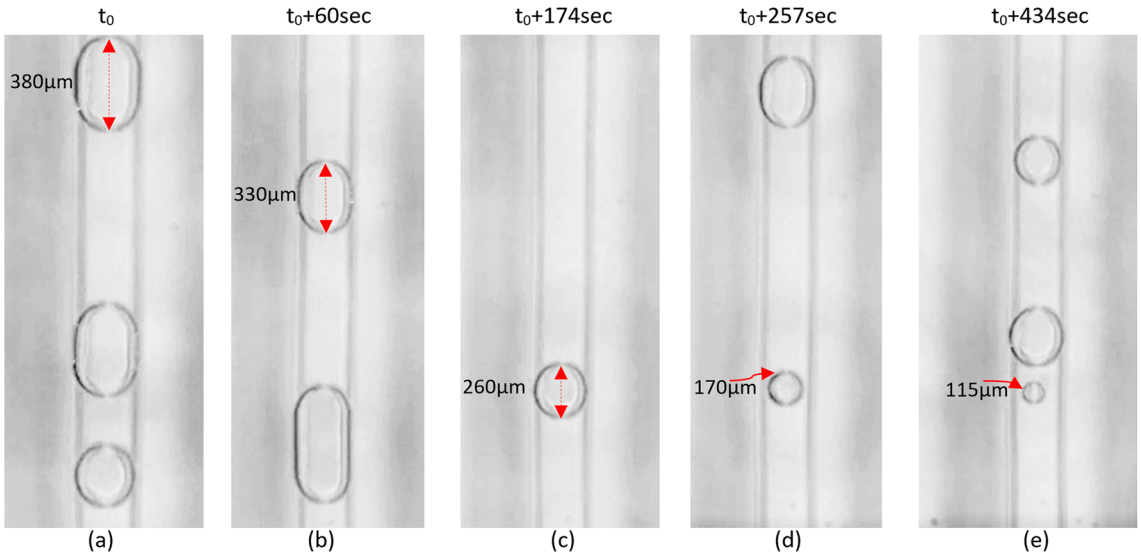

Fig. 7 Dynamics of a bubble (same bubble from a to e) moving within the microchip highlighting CO_2 gas dissolution in water: (a) movement of CO_2 bubble (size 380 µm: red arrow); (b) movement of CO_2 bubble (size reduction to 330 µm); (c–e) gas bubble size reduction *versus* time (260, 170, and 115 µm, respectively).

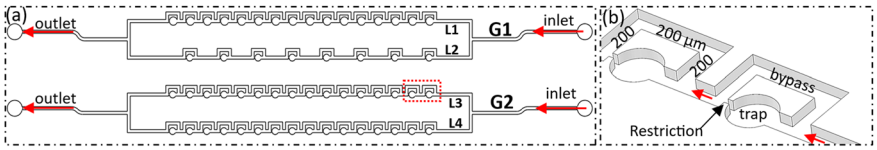

Fig. 8 Prototype droplet-trap micro-chip. The injection's direction is indicated by red arrows. (a) View of the chip exhibiting different lines corresponding to Table 1; (b) view of channel sizes on two highlighted traps (within the red box in (a)).

Procedure to generate droplets/bubbles. This microfluidic chip has a single inlet and a single outlet for each line (Fig. 9a). The main challenge is to generate multiple droplets or bubbles using single-phase flows under pressure. Initially, the channels are filled with water to maintain the pressure (15 bar for CO_2 gas and 50 bar for CO_2 liquid) (Fig. 9b). Once the chip reaches the desired pressure, the water flow is stopped. The first step involves introducing the phase that will form droplets or bubbles (CO_2 liquid or gas) into the chip. The CO_2 fluid pushes the water out of the channels (Fig. 9c). The next step is the introduction of the phase that will stay in the bypass. Water is injected into the channel, which prevents the CO_2 liquid or gas in the trap from being moved because of the channel restriction (50 µm) behind it. The first droplet blocks the channel restriction and seals the exit, and the water then flows through the bypass channel (Fig. 9d). The videos for these procedure steps are available in the ESI† (Annex S1–S9c and S1–S9d). Optimizing the channel sizes and restrictions is crucial. If the restriction size is too large, CO_2 may be pushed out of the trap. The water flow rate at the last step is 5 mL h^{-1}.

Fig. 10 illustrates results for both liquid and gaseous CO_2, showcasing the effectiveness of the trapping mechanism. Notably, the optical observation of CO_2 bubbles in water is better than that of CO_2 liquid droplets.

Final chip design. Following the prototype chip tests, a second chip with the geometry of group 2/line 3 was fabricated. This chip is able to trap 70 droplets/bubbles of CO_2 in either liquid or gas form in water flow or 70 water droplets in either CO_2 gas or liquid flow. Fig. 11 illustrates a schematic view of this chip, including a close-up of a part of the droplet-trap micro-chip for CO_2 droplet/bubble trapping in water flow.

Fig. 12 illustrates the procedure applied to the droplet-trap microchip for water droplets in CO_2 flow. A notable difference from previous methods (Fig. 11a) is a 180 degree clockwise rotation of the chip (Fig. 12a). This rotation, highlighted in the red boxes in Fig. 11a and 12a, changes the 200 µm channel to a 50 µm restriction in the flow direction. Once the chip is pressurized with water, CO_2 is injected to

Table 1 Description of the different lines for the prototype chip as shown in Fig. 8

Group/line	Trap diameter (µm)	Restriction width (µm)	Spacing between traps (µm)
G1/L1	550	50	200
G1/L2	450	50	1400
G2/L3	**450**	**50**	**200**
G2/L4	450	60	200

This journal is © The Royal Society of Chemistry 2025

Open Access Article. Published on 29 april 2025. Downloaded on 05-06-2026 21:04:26.
This article is licensed under a Creative Commons Attribution-NonCommercial 3.0 Unported Licence.

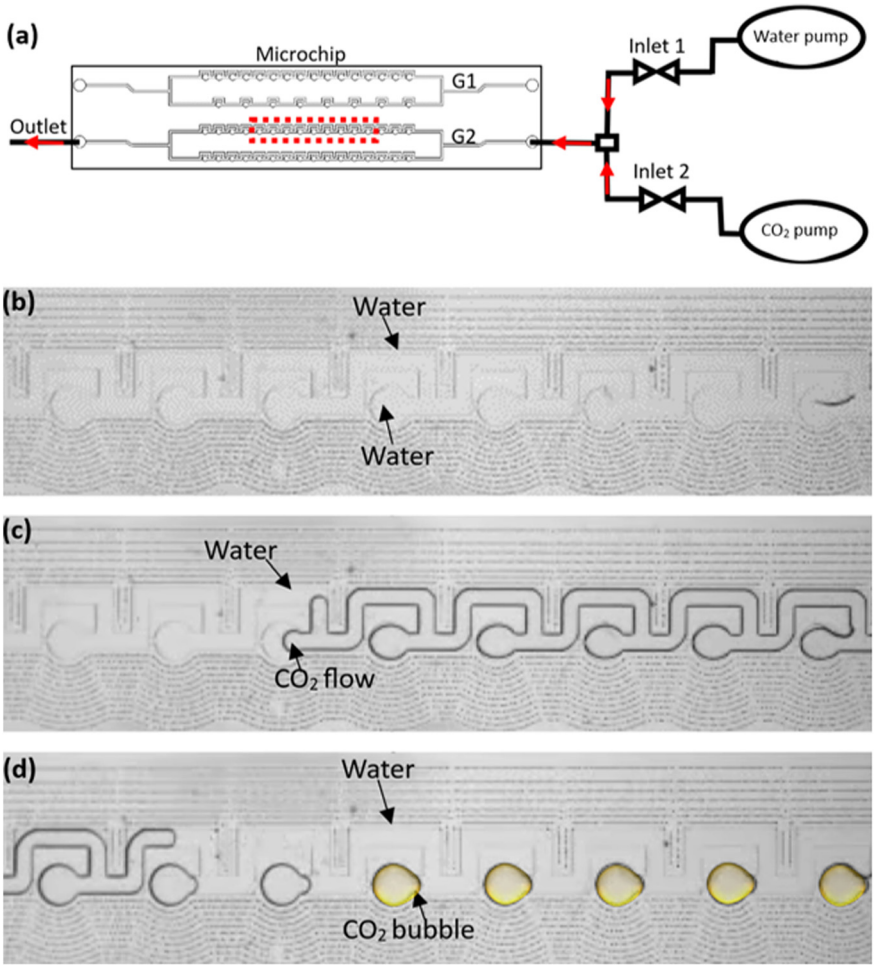

Fig. 9 Procedure to trap CO_2 bubbles: (a) schematic of the microchip, syringe pumps, inlets, and outlets; (b) water injection to maintain the desired pressure; (c) CO_2 injection at the same pressure; (d) water injection.

trap the water droplets. It is necessary to inject with the correct flow rate according to the setup to ensure all droplets are of identical form. For instance, one droplet is smaller than the others (highlighted with a black frame) because the second step of CO_2 injection did not correctly fill it with CO_2.

4. Experimental results

The results for CO_2 hydrate formation on each chip are presented here. It is important to note that the limit of stability for CO_2 hydrate in pure water is 1.7 °C under 15 bar pressure. At 50 bar pressure, the stability limit is −10.2 °C. These results include close-up images to enhance observation of the CO_2 hydrate crystallization onset.

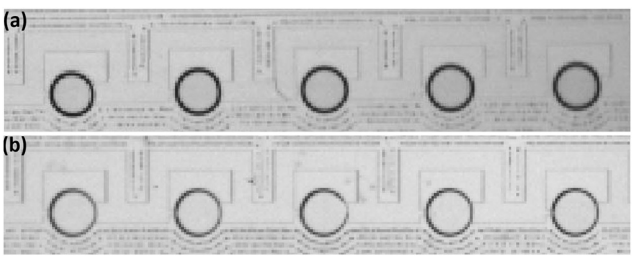

Fig. 10 (a) CO_2 bubbles in water at a pressure of 15 bar, (b) CO_2 droplets in water at a pressure of 50 bar.

4.1. Tests with capillary channel chip (serpentine-shaped)

Fig. 13a shows six CO_2 droplets (liquid phase) in water under a static condition at a pressure of 50 bar, captured at the initial time t_0 (just before the CO_2 hydrate crystallization). Blue arrows indicate the flow direction within the channel during the injection of the two fluids and the droplet generation. Fig. 13b illustrates the crystallization of all droplets at t_0 + 1 s with the crystallized regions marked by red boxes. These regions emphasize that crystallization depends on the flow injection direction; hydrates appear "behind" the droplet, following the flow direction. The crystallization occurs mainly "in front of" the droplets, following the flow direction as highlighted by the red box. Crystallization is also present "behind" the droplets, but with a reduced extent. The length of all droplets is presented for both scenarios (before and following hydrate formation),

Open Access Article. Published on 29 april 2025. Downloaded on 05-06-2026 21:04:26.
This article is licensed under a Creative Commons Attribution-NonCommercial 3.0 Unported Licence.

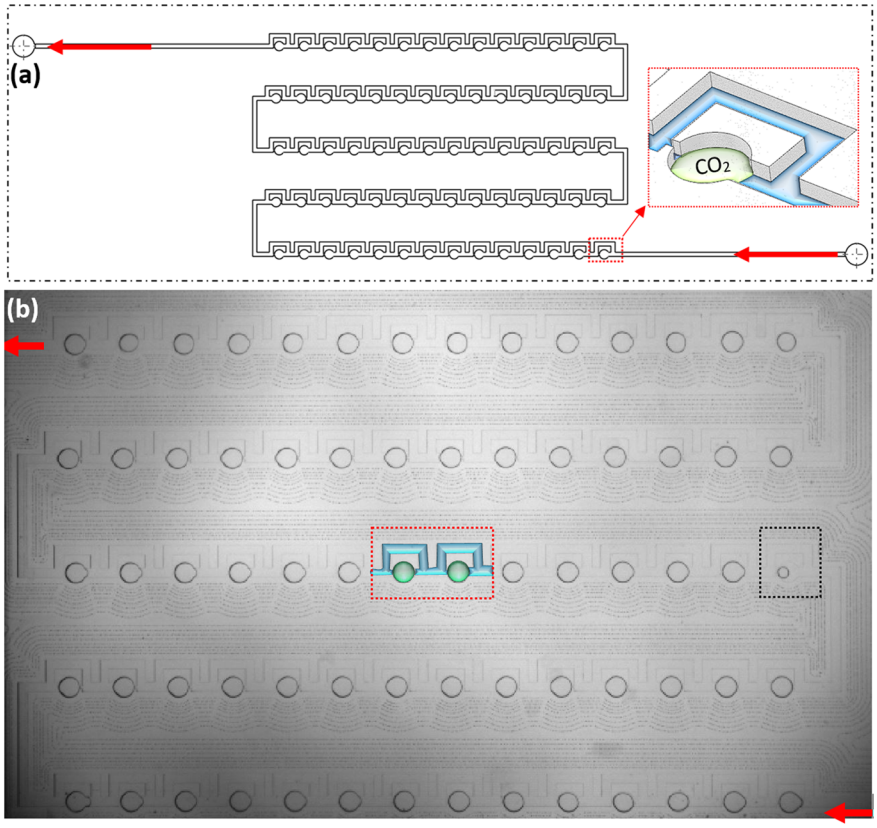

Fig. 11 (a) Schematic view of the final droplet-trap microchip (b) optical view of the microchip displaying a single flow inlet and a single flow outlet (red arrows), through which water flows into the channels. CO_2 droplets are effectively captured within designated trap sites. The storage area is organized into five rows, each containing 14 traps, resulting in a total capacity to store 70 droplets/bubbles.

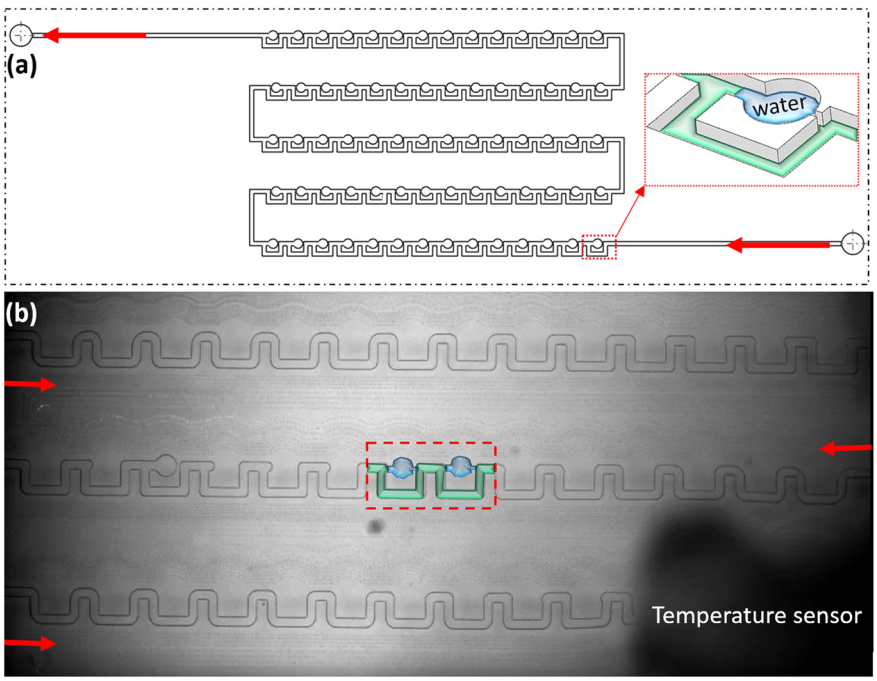

Fig. 12 (a) Schematic view of the droplet-trap microchip rotated 180 degrees clockwise (b) optical view of the microchip showing the CO_2 flow direction (red arrows). Water is effectively captured within designated trap sites.

This journal is © The Royal Society of Chemistry 2025

Open Access Article. Published on 29 april 2025. Downloaded on 05-06-2026 21:04:26.
This article is licensed under a Creative Commons Attribution-NonCommercial 3.0 Unported Licence.

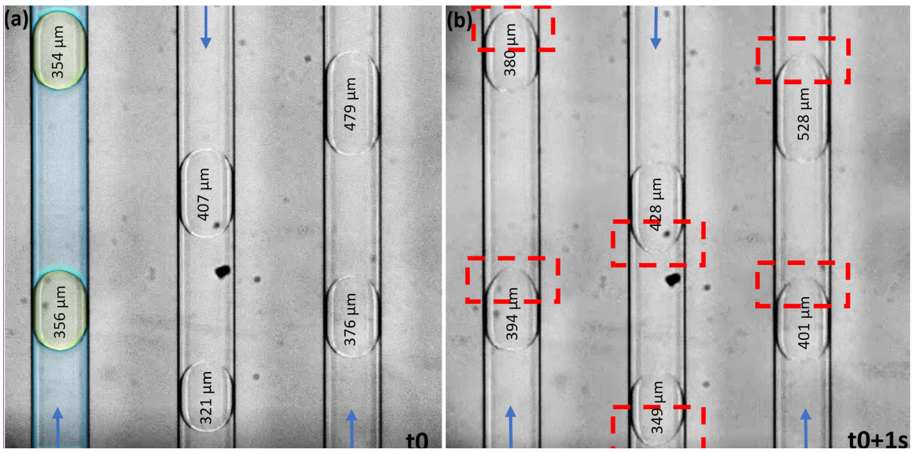

Fig. 13 A close-up view of the CO_2 droplets at 50 bar before (t_0) and after hydrate formation (t_0 + 1 s): (a) CO_2 droplets in water, with the flow direction indicated by blue arrows. One line is colored for a better visualization of conditions, green represents the CO_2 droplets, and blue represents the water; (b) hydrate crystallization zones marked with red boxes.

showing an increase in droplet length. Unlike CO_2 gas, the water/CO_2 liquid interface is less distinct, making it more challenging to observe hydrate crystallisation. Instead of apparent structural changes, hydrate formation is first detected by subtle deformations at the interface. For Fig. 13, supplementary image sequences (from image 1 to image 27) are available, recorded at 5 FPS, with each image representing a time interval of 0.2 s. Black arrows in the images highlight the moment of hydrate crystallization, allowing for comparison between images to better understand the crystallization process.

Fig. 14a shows seven CO_2 bubbles (gas phase) in water under static conditions at a pressure of 15 bar, observed at t_0 (just before the CO_2 hydrate crystallization). Blue arrows indicate the flow direction. Fig. 14b illustrates the crystallization of all CO_2 bubbles at t_0 + 1 s (just after the CO_2 hydrate crystallization), highlighted by red boxes. The crystallization occurs mainly "in front of" the bubbles, following the flow direction as highlighted by the red box. Crystallization is also present "behind" the bubbles, but with a reduced extent. In addition, an increase in the droplet length can be observed. It is important to note that the increase in bubble/droplet length begins immediately after the hydrate formation (t_0 + 1 s). However, depending on the conditions, subsequent hydrate growth can further increase this length. For Fig. 14, supplementary image sequences (from image 1 to image 60) are available, recorded at 5 FPS, with each image representing a time interval of 0.2 seconds. Black arrows in the images highlight the moment of hydrate crystallization, allowing for comparison between images to better understand the crystallization process.

Fig. 15 presents a comparative analysis of the length of CO_2 droplets (liquid phase, green diamonds) and bubbles (gas phase, yellow triangles) before and after hydrate formation. The data points, derived from the observations in Fig. 13 and 14, are plotted against each other, with the x-axis representing the length before hydrate formation and the y-axis representing the length after hydrate formation.

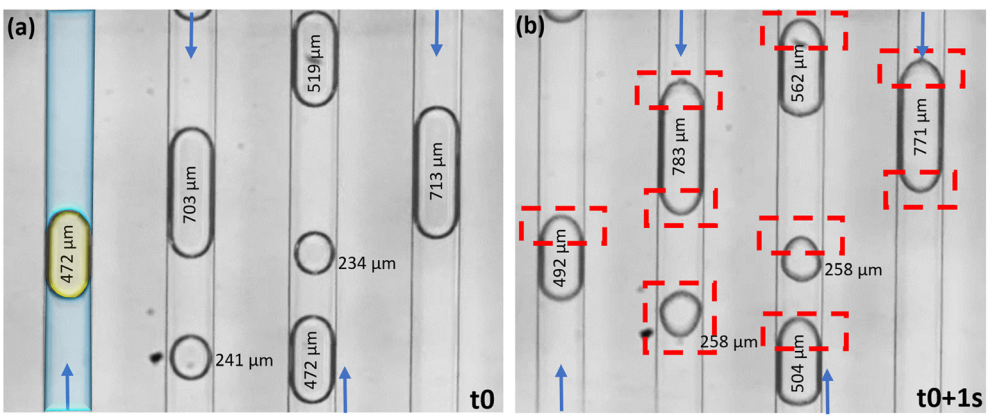

Fig. 14 A close-up view of the CO_2 gas bubbles at 15 bar before (t_0) and after hydrate formation (t_0 + 1). (a) CO_2 bubbles in water with the flow direction indicated by blue arrows. One line is colored for better visualization of conditions: green represents the CO_2 bubbles, blue represents the water; (b) hydrate crystallization, highlighted with red boxes.

Open Access Article. Published on 29 april 2025. Downloaded on 05-06-2026 21:04:26.
This article is licensed under a Creative Commons Attribution-NonCommercial 3.0 Unported Licence.

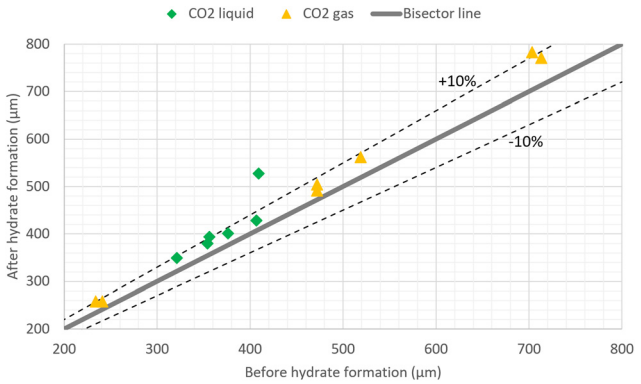

Fig. 15 CO_2 droplet/bubble size variation due to hydrate formation before and after hydrate formation in the capillary channel chip.

Compared to the bisector line, droplet/bubble lengths increase after hydrate crystallization. Dashed lines representing a ±10% deviation from the bisector line are also included to visualize the magnitude of this change.

In the case of CO_2 bubbles, distinct morphologies are observed. This observation primarily serves to optically compare small bubbles with those of different sizes. These morphologies, following crystal growth, are depicted in Fig. 16. The bubble sizes range from 230 μm (Fig. 16e) to 831 μm (Fig. 16b). The morphologies in Fig. 16a–d are quite different from each other, whereas the morphologies of the four bubbles in Fig. 16e, with sizes ranging from 230 to 361 μm, are nearly identical. This suggests that bubble size may influence the final morphology, though further investigation is needed to fully understand the underlying mechanisms.

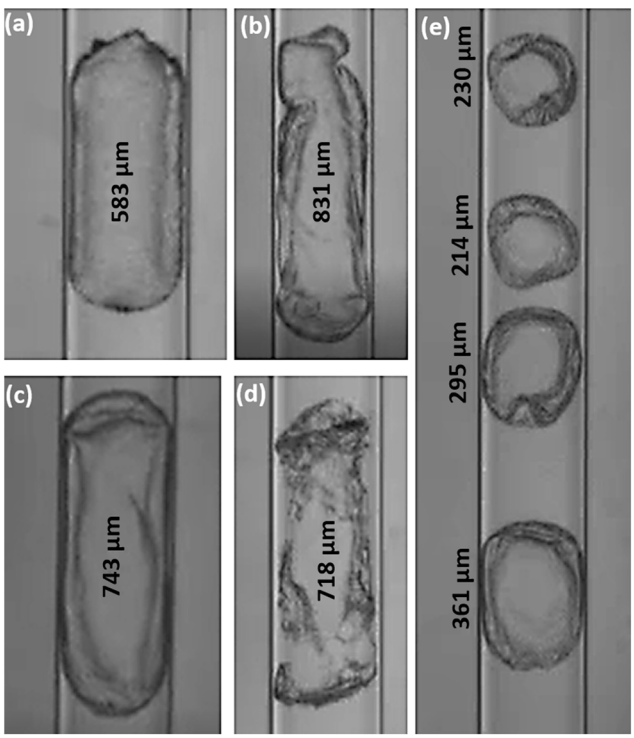

Fig. 16 (a–e) Different morphologies of CO_2 bubbles.

4.2. Test with droplet-trap microchip

The results obtained using the droplet-trap microchip are presented in this section. Fig. 17a–c depict CO_2 bubbles in water at ambient temperature. During this phase, precise control of the water flow rate in the final step is crucial to prevent the deformation of the trapped CO_2 bubbles. Once the trapping process is complete and all bubbles are secured, a decrease in temperature brings the system into the hydrate stability zone. The mutual dissolution of CO_2 and water, combined with the reduction of the molar volume of CO_2, results in a decrease in bubble size. This size reduction is illustrated in Fig. 17d–g. The video of the bubble size evolution is available in the ESI† (Annex S2–S16).

In an alternative procedure, water droplets are trapped while CO_2 is in the channels under either static or dynamic flow conditions. In static conditions, the pumps are turned off once the water droplets are trapped. In the dynamic condition, CO_2 gas or liquid circulates through the loops after trapping the water droplets. In this method, water droplets remain stable and do not undergo dissolution as observed when CO_2 bubbles are trapped. Additionally, under dynamic conditions, the flow rate of CO_2 can be adjusted as

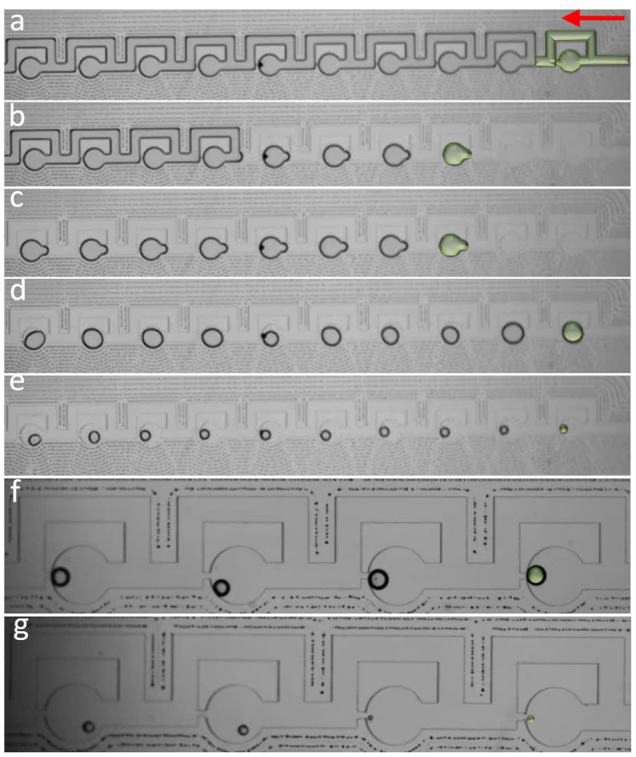

Fig. 17 Results with droplet-trap microchip: (a–c) initial injection of CO_2 followed by water injection to trap CO_2 bubbles; (d–g) bubble size decrease during the subsequent cooling phase (mutual dissolution of CO_2 and water). CO_2 is colored green in the first part of each sub-figure.

This journal is © The Royal Society of Chemistry 2025

Open Access Article. Published on 29 april 2025. Downloaded on 05-06-2026 21:04:26.
This article is licensed under a Creative Commons Attribution-NonCommercial 3.0 Unported Licence.

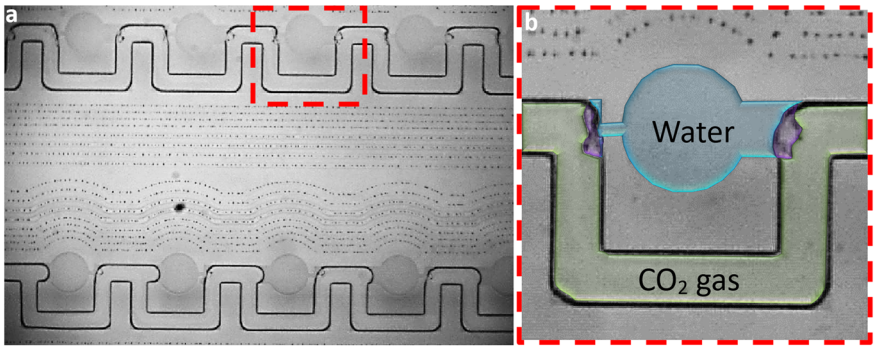

Fig. 18 (a) A close-up view of water trapped with CO_2 gas flow after hydrate formation; (b) an optical zoom of one trap, highlighted with a red box, showing different phases: CO_2 gas in green, water in blue, and CO_2 hydrate crystallization in violet.

needed, providing greater flexibility when using this experimental setup. A case study (Fig. 18), based on numerous tests, demonstrates the feasibility of this method.

Fig. 18a shows a close-up view of the chip under dynamic conditions, with CO_2 gas (at a pressure of 15 bar) injected at a rate of 4 mL h^{-1} (equivalent to a velocity of ~28 mm s^{-1} at the channel). As the temperature decreases, hydrates form at the water–CO_2 gas interfaces. The video of the hydrate formation is available in the ESI† (Annex S3–S17). Fig. 18b provides an optical zoom of one trap (highlighted by a red box), where CO_2 gas flow is depicted in green, water in blue, and hydrate crystallization in violet.

A similar procedure to the one shown in Fig. 17 can be enhanced by introducing an additional step of CO_2 flush. Fig. 19a illustrates the setup at the end of the previous procedure. If CO_2 is injected after this step, it enters the channel while a thin layer of water remains between the CO_2 droplets/bubbles (Fig. 19b). Additionally, small amounts of water remain in the corners of the channels.

5. Discussion

Chip designs play a crucial role in controlling the behavior of CO_2 droplets and bubbles within microfluidic channels. The differences in channel geometry can help to understand their impact on the localization and control of the CO_2/water interface, which is essential to form hydrates in multiple droplets and bubbles. This paper aims to compare CO_2 hydrate formation in two high-pressure microfluidic chips at pressures below 70 bar, the capillary channel chip (serpentine-shaped) and the trap chip, each with specific advantages and limitations when investigating CO_2 hydrate formation. Different procedures are applied to each microchip investigating CO_2 hydrate at the interfaces between liquid water–CO_2 gas or liquid water–liquid CO_2, based on their characteristics. This section discusses the advantages and drawbacks of each chip design for CO_2 bubbles, CO_2 droplets or water droplets.

The capillary channel chip, which is commercially available, does not require design modifications and can generate CO_2 droplets and bubbles. However, generating uniform CO_2 bubbles in water (gas–liquid system) under pressure remains challenging when using a Y-junction droplet generator. Achieving an optimal flow rate balance between the water and CO_2 injections with this Y-junction setup was particularly difficult, resulting in heterogeneous bubbles. Switching to alternative geometries, such as a T-junction, flow-focusing, or co-flow design, can simplify the generation of uniform CO_2 bubbles in water.[8,17,18] In contrast, when using liquid CO_2 (liquid–liquid system) under the same conditions, generating uniform CO_2 droplets in water was significantly more straightforward with this Y-junction droplet generator. Once the droplets or bubbles were generated, movement within the capillary channel was observed during the cooling phase. The movement of droplets/bubbles caused issues such as droplet and bubble displacement, size inconsistencies, and coalescence. A similar movement was also observed during the heating phase when hydrate dissociation occurred. This challenge may be attributed to the movements resulting from

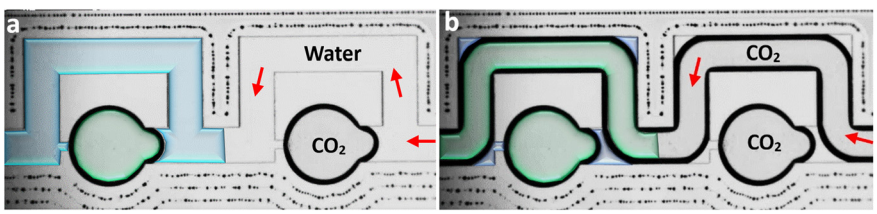

Fig. 19 Comparison of two procedures for trapping CO_2 droplets/bubbles. The left side of each procedure is colored for better visualization: CO_2 is shown in green, and water in blue. Red arrows indicate the flow direction. (a) The procedure is similar to that in Fig. 16. (b) The procedure with an additional step of CO_2 injection.

Open Access Article. Published on 29 april 2025. Downloaded on 05-06-2026 21:04:26.
This article is licensed under a Creative Commons Attribution-NonCommercial 3.0 Unported Licence.

temperature differences between the storage zone and the inlet/outlet lines. Subsequently, the fluid density is affected by this temperature cycle and CO_2 dissolution in brine. However, besides these challenges, this capillary channel is widely applied under dynamic flow conditions to assess mass transfer between CO_2 and brine.[16–18] This capillary channel, sealed at one end, mainly in hydrate application, allowed for observation by focusing on a single droplet or bubble[22,23,25,26] interface. In this study, to address displacement issues, the system was pre-cooled to −10 °C. While complete elimination of movement was not achieved, a quasi-stable state was attained between the cessation of droplet/bubble movement at −10 °C and the initiation of hydrate formation. This quasi-stabilization, characterized by minimal residual movement, facilitated the maintenance of droplets/bubbles within the observation zone. Nevertheless, hydrate growth measurements using this chip revealed an increase in droplet/bubble size after hydrate formation. The scatter plot reveals that for both liquid and gaseous CO_2, the length of the structures increases after hydrate formation. This increase is generally within +10%. It can be attributed to the formation of a solid hydrate layer at the interface between the CO_2 phase and the surrounding water, effectively expanding the overall dimensions of the droplet or bubble. While there is some variability in the extent of this increase, as indicated by the spread of the data points around the bisector line, the overall trend suggests a consistent expansion upon hydrate formation under the tested static conditions at 50 bar for liquid CO_2 and 15 bar for gaseous CO_2.

The trap chip was specifically designed to address droplet and bubble movement issues. It features a multi-loop channel that effectively traps CO_2 droplets, CO_2 bubbles, or water droplets, with two different resistances on either side of the trap area providing a structural trap.[24] This design supports various mixture states, CO_2 droplets/bubbles in water, water droplets in CO_2 (gas or liquid), and double-envelope structures where a water layer surrounds CO_2. In the first procedure, involving CO_2 droplets or bubbles in water, mutual dissolution between CO_2 and water was observed,[27] resulting in a reduction in droplet or bubble size within the trap area, often leading to the loss of bubbles or droplets. This method is highly effective for studying dynamic CO_2 mass transfer. The second procedure, focusing on water droplets in CO_2, proved advantageous for trapping water droplets and CO_2 (gas or liquid) within the loop channels. It minimized droplet size variability, ensuring excellent stability and control during temperature cycles, such as cooling for hydrate formation and heating for dissociation. The final procedure, using double-envelope structures where a water layer encapsulates CO_2, gains insights into hydrate formation on the CO_2–water interface. The unique geometry of the chip enables flexibility for new experimental setups. For instance, injecting water or CO_2 from one side while introducing another fluid from the opposite side allows the creation of novel procedures. This versatility enhances its potential for exploring complex fluid interactions, hydrate formation, and CO_2 mass transfer.

In this context, the capillary channel chip, characterized by its simpler channel geometry, provides limited control over the interface between CO_2 and water. This weak control becomes a significant drawback when dealing with many droplets or bubbles in the channel during hydrate formation. In such cases, maintaining a stable and well-defined CO_2/water interface is critical, particularly during the hydrate formation process, where any instability can lead to inconsistencies in droplet or bubble behavior, reduced efficiency, or failed experiments. In contrast, with its multi-loop channel geometry, the trap chip design is precisely engineered to address these challenges. It provides enhanced trapping capabilities, effectively immobilizing droplets and bubbles while maintaining stable CO_2/water interfaces. This stability is particularly advantageous for hydrate formation as it ensures consistent conditions across all droplets or bubbles in the system. Thanks to its geometry, which includes a bypass channel for each loop, the trap chip enables a novel approach to dynamic flow experiments, offering significant insights into hydrate formation under varying hydrodynamic conditions. The ability of the trap chip to control CO_2 flow through its loops allows for real-time observation of crystallization processes at the water/CO_2 interface. These experiments provided insights into hydrate crystallization, revealing the intricate interplay within each loop, including the consistent detection of hydrate formation at the same point and the interaction zones between water and CO_2. This design also enables the study of the impact of hydrate crystallization in one loop on the behavior and dynamics of other loops.

All the experiments in this work were observed using optical methods. The contrast between CO_2 gas in water was much more apparent than between CO_2 liquid and water. This difference arises from the variation in density between gaseous and liquid CO_2. Unlike CO_2 bubbles, CO_2 droplets are miscible with the aqueous phase. Consequently, the refractive index difference at the interface of gaseous CO_2 bubbles, which behave like solid particles, is more pronounced than that of liquid CO_2, which gradually dissolves into water.[28] This visibility difference is crucial when observing the entire storage zone. The reduced contrast in the case of CO_2 droplets (*i.e.* CO_2 liquid) in water makes detecting the onset of hydrate formation more challenging. As a result, higher optical zoom is required, limiting the number of observable storage zones and CO_2 droplets.

In summary, both chip designs offer distinct advantages and limitations for studying CO_2 hydrate formation. With its simpler geometry, the capillary channel chip is adequate for assessing mass transfer. However, its limited control over the CO_2/water interface, especially when handling multiple droplets or bubbles, can lead to instability and inconsistent results during hydrate formation. In contrast, the trap chip's

 This journal is © The Royal Society of Chemistry 2025

Open Access Article. Published on 29 april 2025. Downloaded on 05-06-2026 21:04:26.
This article is licensed under a Creative Commons Attribution-NonCommercial 3.0 Unported Licence.

multi-loop design is precisely engineered to immobilize droplets and bubbles with consistent spacing between loops. No limitations or challenges were observed in the procedure involving water droplets in CO_2, which is crucial for consistent and reproducible experiments. Furthermore, this procedure can be effectively utilized under static or dynamic flow conditions. The stability of the interface in each loop provides an ideal setup for image analysis, particularly in terms of interface quality for CO_2 gas bubbles in water. This stability also enables advanced experimental techniques, such as Raman micro spectroscopy.

6. Conclusions

A microfluidic system was developed to investigate the formation of CO_2 hydrates in the context of geological CO_2 storage. A high-pressure holder equipped with a Peltier-based cooling system was designed to allow optical observation and be adaptable for various microchips. Two microchips were tested: the first featured a capillary channel chip, while the second comprised 70 traps connected in series. Both configurations enabled the formation of CO_2 (liquid or gas) droplets/bubbles in water or water droplets in CO_2 under high-pressure conditions. CO_2 hydrates were successfully formed by lowering the system temperature while maintaining high pressure. The following key conclusions can be drawn.

In the capillary channel chip, numerous CO_2 droplets or bubbles can be generated within the serpentine geometry comprising 41 meanders. This serpentine design proves particularly useful when the objective is to observe hydrate propagation between droplets or bubbles. However, accessing detailed information from a specific region within this zone necessitates optical zooming, which inevitably leads to the loss of information from other regions during hydrate formation. Moreover, when the goal is to observe a single droplet or bubble to precisely measure hydrate growth, this capillary channel is not suitable, as it cannot maintain the droplet or bubble in a fixed position. Despite these limitations, the capillary chip effectively enables the formation of CO_2 hydrates from CO_2 droplets or bubbles in water under quasi-static conditions. Hydrate formation was visually observed at the interface between hundreds of CO_2 droplets or bubbles and water, allowing for the determination of the onset temperature corresponding to a given degree of supercooling. Furthermore, crystal growth rates (in terms of lateral size) could be measured within small regions under varying experimental conditions. Nonetheless, this approach has limitations. The movement of CO_2 droplets or bubbles in water increases during temperature changes, particularly as the temperature decreases. In summary, this movement keeps the system in a quasi-static state rather than a fully static one.

To address the limitations encountered with the initial chip design, a new trap-chip configuration was developed, incorporating 70 traps connected in series to store either CO_2 droplets/bubbles or water droplets. This chip, due to its specific geometry, offers several advantages. Notably, it provides complete stability for monitoring the hydrate formation process under varying temperatures in a fully static condition. Additionally, it allows for accurate calculation of the water and CO_2 fractions within the chip based on the experimental procedure. Moreover, the known positions of the traps facilitate precise observation using optical microscopy or even Raman spectroscopy. In the context of CO_2 hydrate formation, generating hydrates from CO_2 droplets or bubbles trapped within the chip proved more challenging than storing water droplets in the traps. This challenge is primarily due to the tendency of CO_2 droplets or bubbles to dissolve into the surrounding water during the cooling phase.

Hydrate formation from liquid CO_2 was successful in only a few cases due to two main challenges. First, there is a significant risk of chip rupture under high pressure, mainly because of the 50 μm channel restrictions. Secondly, when liquid CO_2 is trapped and water flows in the channels, hydrate formation occurs within the channels themselves; upon dissociation, the expansion or movement of the hydrates in the channels can damage the chip, further limiting the success rate of the experiments.

Besides, the geometry of the connected traps and channels is advantageous for conducting tests under dynamic conditions. Water can be trapped within the system, while CO_2 can be dynamically injected at an adjustable flow rate. This setup allows for controlled experiments, enabling the study of hydrate formation under varying flow conditions, simulating more realistic and scalable scenarios for CO_2 hydrate behavior. The connected-traps chip system allows hydrate formation in static and dynamic conditions (*i.e.*, constant flow rate) of CO_2 (gas or liquid) or water. However, this paper primarily demonstrates the device's capabilities. Further studies are necessary to fully understand the influence of geometry, flow dynamics, and hydrodynamics on hydrate morphology and growth.

Data availability

DAS have been added to the submission as ESI† materials. The DAS are mp4 films showing the phenomena explained in three different figures of the article. Annex S1–S9c and S1–S9d† correspond to Fig. 9. Annex S2–S16† correspond to Fig. 16. Annex S3–S17† correspond to Fig. 17.

Author contributions

Peyman Dehghani: writing – original draft, methodology, formal analysis, investigation, data curation,

Open Access Article. Published on 29 april 2025. Downloaded on 05-06-2026 21:04:26.
This article is licensed under a Creative Commons Attribution-NonCommercial 3.0 Unported Licence.

conceptualization. Anne Sinquin: writing – review & editing, validation, supervision, methodology, conceptualization, project administration. Nicolas Gland: writing – review & editing. Eric Lécolier: writing – review & editing, resources, methodology, conceptualization Livio Ruffine: writing – review & editing. Anh Minh Tang: writing – review & editing, validation, supervision, methodology, conceptualization.

Conflicts of interest

There are no conflicts to declare.

Acknowledgements

The authors sincerely thank Sylvie Perrin, Physico-Chemistry Technician at IFP Energies Nouvelles, for her invaluable technical assistance and expertise, and Mathieu Olivier, Industrial Designer at IFP Energies nouvelles, for his contributions to the experimental setup design and support in ensuring the research's technical feasibility.

References

1 IEA Greenhouse Gas R&D Program (IEA GHG), Opportunities for Early Application Of CO2 Sequestration Technology, Report Ph4/10, 2002.
2 IPCC, Prepared by Working Group III of the Intergovernmental Panel on Climate Change, *IPCC Special Report on Carbon Dioxide Capture and Storage*, ed. B. Metz, O. Davidson, H. C. de Coninck, M. Loos and L. A. Meyer, Cambridge University Press, Cambridge, United Kingdom and New York, NY, USA, 2005, p. 442.
3 C. Chesnokov, R. Farajzadeh, K. O. K. Prempeh, S. Kahrobaei, J. Snippe and P. Bedrikovetsky, Analytical model for Joule-Thomson cooling under heat exchange during CO2 storage, *Adv. Water Resour.*, 2024, **190**, 104758.
4 H. Hoteit, M. Fahs and M. R. Soltanian, Assessment of CO2 Injectivity During Sequestration in Depleted Gas Reservoirs, *Geosciences*, 2019, **9**, 199.
5 M. Khurana, Z. Yin and P. Linga, A Review of Clathrate Hydrate Nucleation, *ACS Sustainable Chem. Eng.*, 2017, **5**, 11176–11203.
6 Z. Yin, M. Khurana, H. K. Tan and P. Linga, A review of gas hydrate growth kinetic models, *Chem. Eng. J.*, 2018, **342**, 9–29.
7 N. Maeda, *Nucleation of Gas Hydrates*, Springer International Publishing, Cham, 2020.
8 P. Zhu and L. Wang, Passive and active droplet generation with microfluidics: a review, *Lab Chip*, 2016, **17**, 34–75.
9 P. N. Nge, C. I. Rogers and A. T. Woolley, Advances in microfluidic materials, functions, integration, and applications, *Chem. Rev.*, 2013, **113**, 2550–2583.
10 M. Fani, P. Pourafshary, P. Mostaghimi and N. Mosavat, Application of microfluidics in chemical enhanced oil recovery: A review, *Fuel*, 2022, **315**, 123225.
11 C.-X. Zhao and A. P. Middelberg, Two-phase microfluidic flows, *Chem. Eng. Sci.*, 2011, **66**, 1394–1411.
12 Q. Liu, Y. Liu, J. Xu, Y. Teng, Z. Ling, Y. Zhang, L. Jiang and Y. Song, A review of the gas hydrate phase transition with a microfluidic approach, *Energy Rev.*, 2023, **2**, 100011.
13 M. L. M. de Baños, O. Carrier, P. Bouriat and D. Broseta, Droplet-based millifluidics as a new tool to investigate hydrate crystallization: Insights into the memory effect, *Chem. Eng. Sci.*, 2015, **123**, 564–572.
14 P. Dehghani, A. Sinquin, N. Gland, A. M. Tang and A. Estublier, Investigating cyclopentane hydrate nucleation and growth using microfluidics, *Sci. Technol. Energy Transition*, 2023, **78**, 36.
15 S. Marre, A. Adamo, S. Basak, C. Aymonier and K. F. Jensen, Design and Packaging of Microreactors for High Pressure and High Temperature Applications, *Ind. Eng. Chem. Res.*, 2010, **49**, 11310–11320.
16 T.-H. M. Ho, J. Yang and P. A. Tsai, Microfluidic mass transfer of CO2 at elevated pressures: implications for carbon storage in deep saline aquifers, *Lab Chip*, 2021, **21**, 3942–3951.
17 C. Yao, Z. Dong, Y. Zhao and G. Chen, Gas-liquid flow and mass transfer in a microchannel under elevated pressures, *Chem. Eng. Sci.*, 2015, **123**, 137–145.
18 J. Yang and P. A. Tsai, Microfluidic mass transfer of supercritical CO2 in brine, *Chem. Eng. Sci.*, 2024, **300**, 120543.
19 Y. Chen, B. Sun, L. Chen, X. Wang, X. Zhao and Y. Gao, Simulation and Observation of Hydrate Phase Transition in Porous Medium via Microfluidic Application, *Ind. Eng. Chem. Res.*, 2019, **58**, 5071–5079.
20 Y. Ji, J. Hou, E. Zhao, C. Liu, T. Guo, Y. Liu, B. Wei and Y. Bai, Pore-scale study on methane hydrate formation and dissociation in a heterogeneous micromodel, *J. Nat. Gas Sci. Eng.*, 2021, **95**, 104230.
21 X. Li, C. Wang, Q. Li, Q. Fan, G. Chen and C. Sun, Study on the Growth Kinetics and Morphology of Methane Hydrate Film in a Porous Glass Microfluidic Device, *Energies*, 2021, **14**, 6814.
22 H. T. Le Goff, F. Lagarde, M. Bousqué and E. Santanach-Carreras, A Microfluidic Experimental Approach to Access CO2 Hydrate Risk for CO2 Storage into Depleted Reservoirs, Proceeding at "16th International Conference on Greenhouse Gas Control Technologies, GHGT-16" held in Lyon, October 23–27th 2022.
23 A. Touil, D. Broseta, N. Hobeika and R. Brown, Roles of Wettability and Supercooling in the Spreading of Cyclopentane Hydrate over a Substrate, *Langmuir*, 2017, **33**, 10965–10977.
24 D. Radajewski, "Etudes de nucléation de protéines à l'aide de dispositifs expérimentaux microfludiques", *PhD thesis*, INPT, Toulouse, 2017, https://oatao.univtoulouse.fr/19317/1/RADAJEWSKI_Dimitri.pdf.
25 A. Touil, D. Broseta and A. Desmedt, Gas Hydrate Crystallization in Thin Glass Capillaries: Roles of Supercooling and Wettability, *Langmuir*, 2019, **35**, 12569–12581.
26 B. Samar, S. Venet, A. Desmedt and D. Broseta, Growth Kinetics and Porous Structure of Surfactant-Promoted Gas Hydrate, *ACS Omega*, 2024, **9**, 31842–31854.

This journal is © The Royal Society of Chemistry 2025

Open Access Article. Published on 29 april 2025. Downloaded on 05-06-2026 21:04:26.
This article is licensed under a Creative Commons Attribution-NonCommercial 3.0 Unported Licence.

27 M. Aghajanloo, L. Yan, S. Berg, D. Voskov and R. Farajzadeh, Impact of CO2 hydrates on injectivity during CO2 storage in depleted gas fields: A literature review, *Gas Sci. Eng.*, 2024, **123**, 205250.

28 P. Luty, M. Prończuk and K. Bizon, Experimental verification of different approaches for the determination of gas bubble equivalent diameter from optical imaging, *Chem. Eng. Res. Des.*, 2022, **185**, 210–222.